In Vivo Computation for Tumor Sensitization and Targeting at Different Tumor Growth Stages

Shaolong Shi[1,2], Yifan Chen[3,4,5], Zheng Gong[4], Xiaoyou Lin[4], Neda Sharifi[4] and Xin Yao[2]

[1]*Harbin Institute of Technology, Harbin, China*
[2]*Department of Computer Science and Engineering, Southern University of Science and Technology, Shenzhen, China*
[3]*University of Electronic Science and Technology of China, Chengdu, China*
[4]*School of Engineering, University of Waikato, Hamilton, New Zealand*
[5]*School of Information Engineering, Putian University, Putian, China*
E-mail: yifan.chen@uestc.edu.cn

***Abstract*—We look into the novel paradigm of *in vivo* computation for tumor sensitization and targeting (TST), which aims at detecting a tumor by considering TST as a computational process. Nanorobots are utilized as computational agents to search for the tumor in the high-risk tissue with the aided knowledge of the tumor-triggered biological gradient field (BGF), which is similar to an optimization process. All our previous work is about the detection of tumor with *a priori* size, which is not convincing enough as the exact size of the tumor targeted cannot be obtained in advance. We focus on the TST for tumor with unknown size by considering the tumor growth process in this paper. The weak priority evolution strategy (WP-ES) based *in vivo* computational algorithm proposed in our previous work is utilized for the TST at three tumor growth stages for two representative landscapes by considering the nanorobots' lifespans and other realistic constraints. Furthermore, we propose the "tension and relaxation (T-R)" principle, which is used for the actuating of nanorobots in the TST process for the tumor with unknown size. The experimental results demonstrate the effectiveness of the proposed *in vivo* computational algorithm and principle for the TST at different tumor growth stages.**

***Index Terms*—Tumor sensitization and targeting, *in vivo* computation, nanorobots, tumor growth stages, swarm intelligence algorithm**

I. Introduction

Although the overall cancer mortality has declined in the past few decades, it is still a great challenge to achieve accurate detection of early cancer because of the constraint imposed by the poor resolution of traditional medical imaging techniques [1], [2]. It is important to find new ways to realize early-stage cancer detection as it plays a vital role in the cure of cancer.

With the development of nanotechnology, the nanomedicine field has shown great potential in providing some breakthrough solutions to complex medical problems that conventional techniques cannot overcome. Nanorobots are designed to be nano-scale devices capable of actuation, sensing, signaling etc., and they are promising to significantly enhance the performance of tumor targeting [3]. Though many different kinds of nanorobots have been developed with distinct actuation principles in the past few decades, fuel-free magnetic nanorobots actuated by external magnetic fields have shown promise for *in vivo* application as it has been proven practicable to realize the *in vivo* imaging and actuation of a swarm of magnetic nanorobots under rotating magnetic fields in deep tissues [4]. However, it is a challenge to realize tumor sensitization and targeting (TST) for microscopic tumors as their location information cannot be obtained *a priori* because of the resolution limit of medical imaging equipments [5].

To overcome the problem of TST for microscopic tumors, we have proposed the nanorobots-oriented *in vivo* computation framework in our previous work [6], [7]. It has been demonstrated that the cancer cells and their local microenvironments will become heterogeneous even at very early stages of tumor growth. Small (< 1 mm) tumor nodules and microregions of larger tumors can be considered as microecological niches where some biological gradients can be generated, such as certain critical metabolites (e.g., oxygen, glucose, lactate, and H^+ ions), nutrients, hormones, and growth factors, etc. [8]. Furthermore, some passive physical properties (tumor vessels are more tortuous than normal capillaries, and their blood flow velocity is lower than that of healthy tissues, etc.) of the host environment and artificial changes of tumor microenvironment triggered by specific "activator" nanomaterials (e.g., gold nanorods) can also be used as *in vivo* characteristics of malignant tissues [7]. Thus, it is feasible to exploit these specific microenvironments (i.e., biological gradient fields (BGFs)) in order to enhance TST for microscopic tumors by *in vivo* computation.

In the *in vivo* computation system shown in Fig. 1, nanorobots play the role of computational agents in the traditional optimization setting, and the tumor-triggered BGF is used for fitness evaluation of the nanorobots, which are navigated by the *in vivo* navigating strategies to find the tumor (i.e., the global maximum or minimum of the *in vivo* optimization problem). Nanorobots are actuated by an external control/actuating system, such as a coil that can generate a uniform rotating magnetic field to steer the magnetic nanorobots in fluid [9]. To locate the nanorobots, traditional imaging equipment can be used [10]. Following this process, each nanorobot will move towards the tumor step-by-step aided by the knowledge (i.e., BGF) about the tumor and stop at the target when it finishes the TST.

As the external control systems are aiming at generating a uniform magnetic field to control the movement of all

978-1-7281-6929-3/20/$31.00 ©2020 IEEE

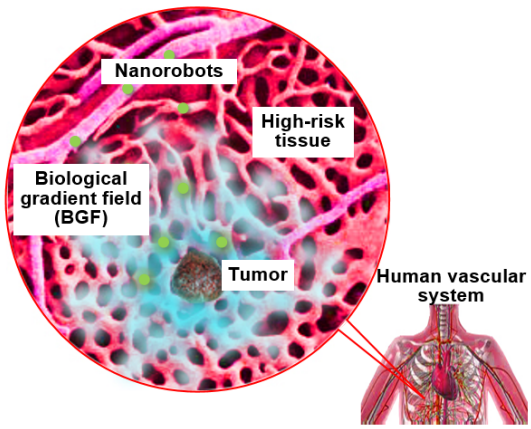

Fig. 1. Pictorial illustration of the nanorobots-oriented *in vivo* computation for TST.

the nanorobots at any operating moment, it is inevitable to consider the effect of the homogeneous magnetic field acting on the nanorobot swarms. Thus, we proposed a novel evolution strategy, named weak priority evolution strategy (WP-ES), to overcome the constraint of the state-of-the-art nanorobotics controlling technology [11]. However, the previous work is focusing on the TST for tumor with *a priori* size (e.g., the tumor radius is assumed to be 0.25 mm in [11]) leaving the topic of TST for tumor with unknown size unstudied. As the latter reflects the fact that the real size of early tumor cannot be obtained before the implementation of TST, it is reasonable to do some research on this topic, which is just the starting point of this paper.

This article is organized as follows. In Section II, we revisit the modeling of *in vivo* computation, summarize its characteristics and provide two artificial representative functions of BGFs. In Section III, we analysis the growth of microscopic tumor vessels and model the tumor vascular networks at three tumor growth stages. In Section IV, we analysis the process of TST and propose the T-R principle for *in vivo* computation. In Section V, the T-R principle based *in vivo* computational algorithm is developed. In Section VI, we provide numerical examples to demonstrate the effective of the proposed algorithm for TST at different tumor growth stages. Finally, some concluding remarks are drawn in Section VII.

II. Fundamentals of *In Vivo* Computation

To establish the framework of *in vivo* computation, we map the process of TST to a min/maximization problem with the tumor being the min/maximum required. However, *in vivo* computation has its own characteristics, which make it different from the mathematical optimization problem though they share some similar procedures.

A. Problem Formulation

In the nanorobots-oriented *in vivo* computation process, each nanorobot is controlled by an external control/actuating device according to the BGF value measured at its location, which is acquired by the external tracking/positioning system. Each nanorobot updates its location step by step until the stopping criteria (it detects the tumor or the maximum number of iterations is reached) are met. This process can be expressed as an optimization problem as below (for consistency and without loss of generality, we use the minimization operation) [7]:

$$U(\boldsymbol{x};A) = U_{\mathrm{T}}(\boldsymbol{x}) + \epsilon(\boldsymbol{x};A) \tag{1}$$

and

$$\boldsymbol{x}^* = \arg\min_{\boldsymbol{x}} U(\boldsymbol{x};A), \tag{2}$$

where U is an *apparent* objective function measured by agent A; $\boldsymbol{x} \in \mathbb{P}$ is a vector to be adjusted (i.e. the agent position coordinate), and $\mathbb{P}$ is the search space of the agents; $U_{\mathrm{T}}(\boldsymbol{x})$ is the *true* objective function, which is unaffected by the agents; $\epsilon(\boldsymbol{x};A)$ is the random compensation error; $\boldsymbol{x}^*$ is the location of the global optimal solution that remains unchanged in the optimization process.

B. Characteristics of In Vivo Computation

Unlike a traditional optimization problem, the nanorobots-oriented *in vivo* computation has several peculiar properties in the process of TST.

In term of the BGF landscape, it may be altered because of some physical, chemical, and biological interactions between the nanorobots and the tissue microenvironment as the nanorobots are always fabricated with natural materials to ensure their functionality. The *in vivo* computation is executed by nanorobots in the human microvascular network, which is a discrete search space. This constraint means that the BGF landscape should be discrete, and it is an inevitable factor for the *in vivo* computation process.

In term of the agents (nanorobots), firstly, their moving speeds in fluid environments are always finite [9]. This is different from the traditional optimization process, where each agent can move to any location in one step instantaneously according to the search strategy used. Secondly, the nanorobots are actuated by a common actuating field in every iteration at the same time, which has been studied in our previous work [11]. Thirdly, the control accuracy and imaging resolution of the external devices may introduce some errors in each update of the nanorobot locations. Furthermore, with the search progressing, some nanorobots may diffuse and degenerate in the tissue microenvironment leading to their "out of work" in the TST process. These factors can be summed up as the finite lifespans of agents.

C. Representation of BGFs

BGFs induced by the tumor can be used to derive biological cost functions for the *in vivo* computation. As there are no widely-accepted, quantitative models of the biological cost functions in this initial research stage, we resort to two representative artificial landscapes (as shown in Fig. 2) in this paper to perform *in vivo* computation as these functions have

been routinely applied in almost all catalogs of standard test problems. The circular region with an unknown radius (i.e., r) in the center of each landscape denotes the tumor targeted.

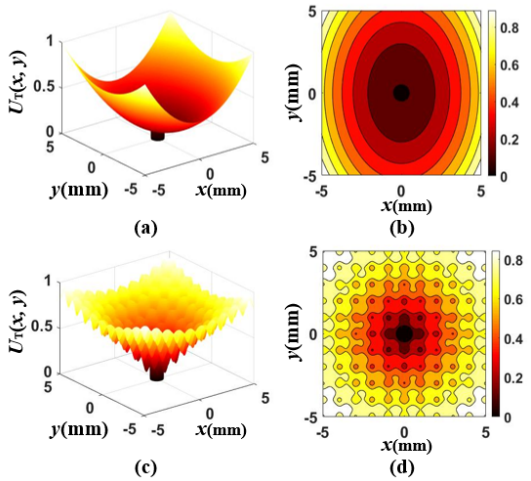

Fig. 2. Illustration of the two representative BGF landscapes. (a) Landscape 1: Rotated Hyper-Ellipsoid Function and (b) its contour plot; (c) Landscape 2: Ackley Function and (d) its contour plot.

1) Landscape 1: Rotated Hyper-Ellipsoid Function

$$U_{\mathrm{T}}(x,y)=\begin{cases}0, & \sqrt{x^2+y^2}\le r \text{ and } (x,y)\in\mathbb{V}\\ \left(x^2+y^2+10\right)/85, & \\ & \sqrt{x^2+y^2}>r \text{ and } (x,y)\in\mathbb{V}.\end{cases} \tag{3}$$

2) Landscape 2: Ackley Function

$$U_{\mathrm{T}}(x,y)=\begin{cases}0, & \sqrt{x^2+y^2}\le r \text{ and } (x,y)\in\mathbb{V}\\ -4\exp\left(-\sqrt{2x^2+2y^2}/10\right)/3+e/15 & \\ +4/3-\exp\left(1/2\left(\cos\left(2\pi x\right)\right)/15\right. & \\ +\cos\left(2\pi y\right), & \sqrt{x^2+y^2}>r \text{ and } (x,y)\in\mathbb{V}.\end{cases} \tag{4}$$

The term $\mathbb{V}$ denotes the discrete vascular network (shown in Section III) in the high-risk tissue, which is the search domain of the nanorobots. The Rotated Hyper-Ellipsoid function and Ackley function represent the scenarios that BGFs change smoothly and with fluctuation, respectively.

III. Tumor Vascular Networks at Different Tumor Growth Stages

The vasculature within early tumors is similar with normal vessel except that it may exhibit a little regression. Angiogenesis occurs in tumors that have reached 1 to 2 mm in diameter when tumor vessels develop by sprouting or intussusception from pre-existing vessels. As the tumor grows, the vasculature within the core of tumor will undergo dramatic regression and the center of tumor will be bereft of vessels gradually. However, the tumor periphery will display robust angiogenesis as a contrast [12].

To describe tumor vascular network, fractal analysis is always used as it can reduce the network to a set of number (known as fractal dimensions) to describe the self-similar nature of the network. The fractal dimension measurements in tumor vasculature indicate that it has a percolation-like nature, which is a local growth process [13]. Thus, we can use invasion percolation to model the growth process of tumor vascular network as shown in [14].

In Fig. 3(a), the tumor at stage I is represented by a black dotted circle with the diameter of 0.6 mm, where the vessel regression results in 30% deprivation of vessels. In Fig. 3(b), the tumor at stage II has a diameter of 1 mm and the vessels are regressed by 40%. Angiogenesis occurs in the tumor periphery represented by a square with a side length of 1.4 mm. In Fig. 3(c), the tumor at stage III has a diameter of 1.4 mm with 50% of vessels regression, and the vessels regression also extends to the tumor periphery with a ratio of 30%. Then angiogenesis extends to the surrounding healthy tissue represented by a square with a side length of 3 mm. Furthermore, the intercapillary distances of healthy tissue and tumor periphery are set to be 100 μm and 50 μm, respectively.

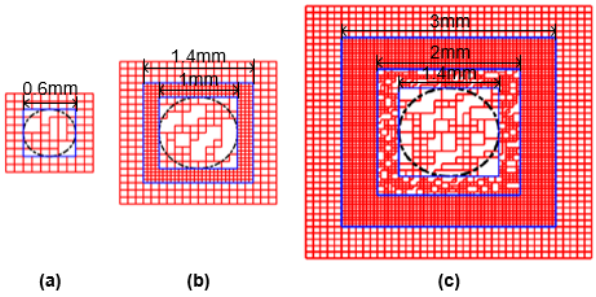

Fig. 3. Vascular networks at three tumor growth stages. (a) stage I (only vessel regression occurs); (b) stage II (vessel regression and angiogenesis both occur); (c) stage III (vessel regression and angiogenesis are both enhanced).

IV. Iterative Process of TST

In the computational framework of TST, nanorobots are maneuvered by an external actuating system to operate in the mode of intended actuating (IA) or unintended actuating (UA). Then the external tracking system makes them operate in imaging and tracking (IT) mode [7]. For the IA/UA mode, each agent's trajectory is determined by the angle deviation relative to a principal axis denoting an intended steering vector upon the agent, which indicates a uniform actuating field in the search space. Without loss of generality, we take agent A_1 as an example and its initial location is $\vec{x}_1\left(t_{\mathrm{IA},1}\right)$ as shown in Fig. 4(a).

From $t_{\mathrm{IA},1}$ to $t_{\mathrm{IT},1}$, A_1 works in the IA mode, which is the UA mode for the other agents. $\varphi\left(t_{\mathrm{IA},1}\right)$ denotes the steering direction, and $\Delta\varphi\left(t_{\mathrm{IA},1}\right)$ denotes an angle deviation, which is a random variable summarizing all steering imperfections and it is assumed to be normally distributed with variance $\sigma^2_{\Delta\varphi}$ and zero mean. $\vec{e}_1\left(t_{\mathrm{IA},1}\right)$ is the position "quantization" error due to the discrete lattice pattern of the vasculature. As described in [7], the vascular network is of taxicab geometry, which means $\|\vec{d}_1\left(t_{\mathrm{IA},1}\right)+\vec{e}_1\left(t_{\mathrm{IA},1}\right)\|_1=\|\vec{d}_1\left(t_{\mathrm{IA},1}\right)\|_1$.

From $t_{\mathrm{IT},1}$ to $t_{\mathrm{IA},2}$, A_1 works in the IT mode. In this mode, there is no steering force on the agents and A_1 follows a random walk in the lattice. Its location in the search space is estimated by the external tracking system with an error of $\Delta\vec{x}_1$, whose horizontal and vertical components are assumed to be independently and identically distributed Gaussian with variance $\sigma^2_{\Delta x}$ and zero mean for simplicity.

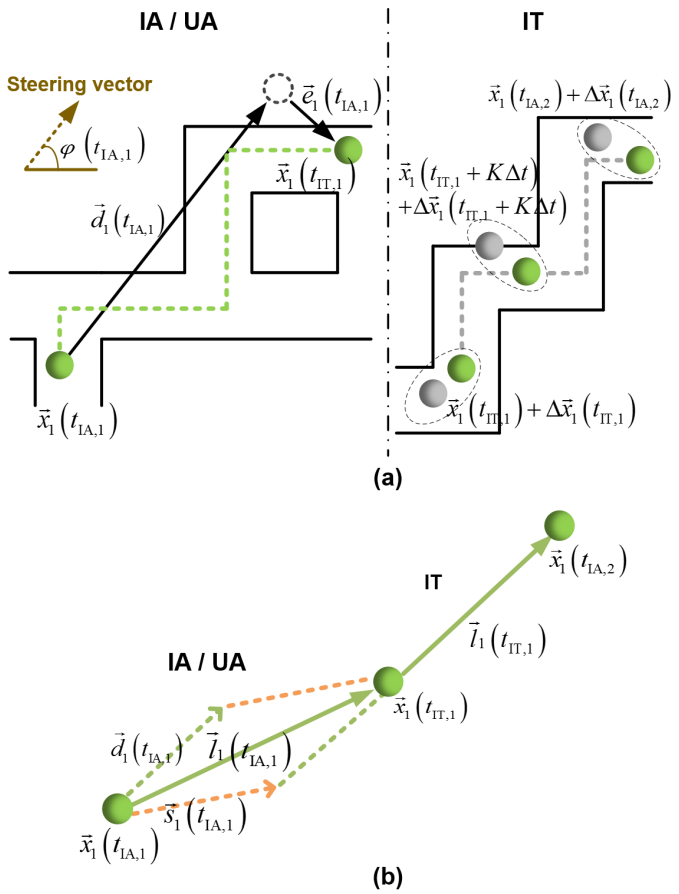

Fig. 4. Updating of a nanorobot in the taxicab vascular network. (a) The processes of IA/UA and IT; (b) T-R principle in the process of TST.

Though our previous work demonstrated the effectiveness of the proposed WP-ES for TST, the most efficient scheduling mechanism for the tumor with unknown size under this umbrella remains unstudied. Thus, we attempt to overcome this issue by exploring the displacements of nanorobots in the IA/UA and IT modes in each iteration, as the process of TST is composed of these two motion modes.

The push-pull theory is the most important macroscopic theory in demography in terms of studying the causes of population mobility, where the factors that help to improve living conditions into the land are the "tension", and the unfavorable living conditions of the outflow are the "thrust" [15]. These two forces cause the population movement aiming at improving living conditions. Inspired by this phenomenon, we propose the "tension and relaxation (T-R)" principle in the process of TST. It means that the effects of IA/UA and IT modes on the displacements of nanorobots should maintain a certain balance to give rise to an optimal performance of TST.

To clarify, the interferences of TST are not taken into consideration in this part, and the velocity magnitude of nanorobots caused by the external actuating field (denoted by $\vec{v}_a$) and the magnitude of blood velocity denoted by $\vec{v}_b$ are assumed to be constants in all the IA/UA and IT modes. As shown in Fig. 4(b), agent A_1 moves from $\vec{x}_1(t_{\mathrm{IA},1})$ to $\vec{x}_1(t_{\mathrm{IT},1})$ with the displacement length of $\|\vec{l}_1(t_{\mathrm{IA},1})\|_1$ in the taxicab vascular network in the first IA/UA mode. Subsequently, it moves from $\vec{x}_1(t_{\mathrm{IT},1})$ to $\vec{x}_1(t_{\mathrm{IA},2})$ with the displacement length of $\|\vec{l}_1(t_{\mathrm{IT},1})\|_1$ in the IT mode. As $\vec{l}_1(t_{\mathrm{IA},1})$ is caused by $\vec{v}_a$ and $\vec{v}_b$, it can be decomposed into $\vec{s}_1(t_{\mathrm{IA},1})$ and $\vec{d}_1(t_{\mathrm{IA},1})$. Thus, the T-R principle proposed can be expressed as

$$\|\vec{s}_1(t_{\mathrm{IA},1})\|_1 + \|\vec{d}_1(t_{\mathrm{IA},1})\|_1 = \|\vec{l}_1(t_{\mathrm{IT},1})\|_1 \tag{5}$$

or

$$(v_a + v_b)\cdot \mathrm{T}_1 = v_b \cdot \mathrm{T}_2, \tag{6}$$

with T_1 and T_2 being the IA/UA and IT durations, respectively.

V. Algorithm Design

Swarm Intelligence inspired by the swarming, flocking and herding phenomena of biological systems is a distributed intelligent paradigm for solving optimization problems. In this paper, we use the WP-ES based GSA (WP-GSA) proposed in [11] as a representative *in vivo* computational algorithm to demonstrate the effectiveness of the T-R principle proposed for TST at different tumor growth stages.

In this algorithm, each agent is considered as an object with its performance being represented by the virtual mass. The position of the agent corresponds to a solution of the problem and its virtual mass is determined by its fitness. All the objects attract each other by their virtual gravity forces and the external actuating system control the movement of agents according to the WP-ES, which will cause a global movement of them towards the optimal solution.

In an *in vivo* computation system with N nanorobots (agents) whose positions are denoted by $\{\vec{x}_1, \vec{x}_2, \cdots, \vec{x}_N\}$, the virtual masses are calculated by

$$\begin{cases} m_i(t) = \dfrac{fit_i(t) - worst(t)}{best(t) - worst(t)} \\ M_i(t) = \dfrac{m_i(t)}{\sum_{j=1}^{N} m_j(t)}, \end{cases} \tag{7}$$

where $i = 1, 2, \cdots, N$, $fit_i(t)$ represents the fitness of agent $\vec{x}_i$, $worst(t)$ and $best(t)$ are defined as follows

$$\begin{cases} best(t) = \max_{i\in 1,2,\cdots,N} fit_i(t) \\ worst(t) = \min_{i\in 1,2,\cdots,N} fit_i(t). \end{cases} \tag{8}$$

The force acting on agent $\vec{x}_i$ from $\vec{x}_j$ is defined as

$$\vec{F}_{ij} = G(t)\frac{M_i(t)\times M_j(t)}{R_{ij}(t)+\varepsilon}\left(\vec{x}_j(t) - \vec{x}_i(t)\right) \tag{9}$$

and

$$G(t) = G_0 \times \mathrm{e}^{-\alpha t/T}, \tag{10}$$

where $R_{ij}(t)$ is the Euclidean distance between $\vec{x}_i$ and $\vec{x}_j$; ε is a small constant; $G(t)$ is the gravitational constant reducing with time; G_0 is set to 10; α is set to 5; and T is the maximum operation time. To obtain a stochastic characteristic, the joint force acting on $\vec{x}_i$ is defined as

$$\vec{F}_i(t) = \sum_{j=1, j\neq i}^{N} rand_j \vec{F}_{ij}(t), \tag{11}$$

where $rand_j$ is a random number in the interval $[0, 1]$. Then the acceleration of agent $\vec{x}_i$ at time t is calculated by

$$\vec{a}_i(t) = \frac{\vec{F}_i(t)}{M_i(t)}. \tag{12}$$

The evolution equations of agents (nanorobots) for *in vivo* computation (i.e., WP-GSA) are as follows
IA / UA mode

$$\begin{cases} \vec{v}_i(t+1) = k\vec{a}_j(t) / \left\|\vec{a}_j(t)\right\|_2 \\ \vec{x}_i(t+1) = \vec{x}_i(t) + \mathrm{T}_1 \cdot (\vec{v}_i(t+1) + \vec{v}_b(t+1)). \end{cases} \tag{13}$$

IT mode

$$\vec{x}_i(t+1) = \vec{x}_i(t) + \mathrm{T}_2 \cdot \vec{v}_b(t+1), \tag{14}$$

where $\vec{v}_b(t+1)$ is the blood flow velocity at time $(t+1)$; $\vec{a}_j(t)$ is the acceleration of the selected agent by WP-ES at time t; k is the speed of nanorobots actuated by the external actuating field solely; T_1 is the IA / UA duration, and T_2 is the IT duration.

VI. Performance Analysis

We use several numerical examples to elaborate on the TST performance at three tumor growth stages with WP-GSA, which is compared to the benchmarking scenario (i.e., the brute-force search), and demonstrate the effectiveness of the T-R principle proposed.

In the simulation, 12 agents with lifespans obeying exponential distribution (i.e., $\tau(A) \sim \mathrm{Exp}\left(5 \times 10^{-4}\right)$) are employed in the surveillance region, -5 mm $\leq x, y \leq$ 5 mm. The initial deployment region is $x \in [-5, -4], y \in [-4, -3]$, within which the initial positions of the agents are uniformly generated. The speeds of nanorobots and blood flow velocity are 30 μm/s. The direction of blood flow is assumed to be from bottom left to top right of the search space. The durations of IA / UA mode (i.e. T_1) and IT mode (i.e. T_2) are set to be 20 seconds. The maximum search time allowed and the number of simulation runs are set to be 500 seconds and 1000, respectively. Two performance metrics η and P_d are used to represent the efficiency of TST (i.e., the ratio of the amount of agents completing TST to the amount of agents deployed and the ratio of the number of tumor targeted successfully to the total number of simulations).

For the benchmarking scenario, the agents detect the tumor in the vascular network relying on the driving of blood flow without any aided knowledge generated from the interaction between agents and the BGFs.

Fig. 5(a) shows the typical curves of the employed agents' average fitness over iterations for the rotated hyper-ellipsoid function landscape at tumor growth stage I by two different search strategies: the brute-force search and WP-GSA. The average fitness of agents relying on WP-GSA reaches the maximum at 250 s and it is higher than that of agents relying on the brute-force search in the whole process of TST, which means that WP-GSA performs better than the brute-force search for this scenario. After 500 seconds, the final locations of the agents in the search space are shown in Fig. 5(b), where we can see WP-GSA can effectively target the tumor with many agents swarming around the tumor, while the performance of brute-force search is not so good with many more agents flowing away. To illustrate it better, we present the trajectories of the agent swarm centers, from which we can see the trajectory of WP-GSA passes through the tumor while that of the brute-force search can only bypass the tumor.

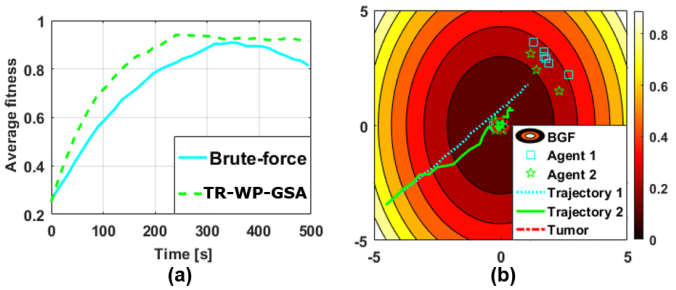

Fig. 5. TST result for landscape 1 at tumor growth stage I. (a) Average fitness of the agents input over iterations, (b) Final locations of agents input in the search space after one run: Agent 1 is the brute-force search agent; Agent 2 is the WP-GSA agent; Trajectory 1 and 2 are the trajectories of the swarm centers of agent 1 and 2, respectively.

TABLE I
TST results at three tumor growth stages

Landscape	Algorithm	Tumor Growth Stage (η / P_d (%))		
		I	II	III
1	WP-GSA	22.4 / 94	58.6 / 99.8	78.3 / 100
2		21.6 / 92	54.7 / 99.2	77.8 / 100
1&2	Brute-force search	10.5 / 72.1	22.6 / 96.4	30.4 / 98

To compare the search algorithms quantitatively, we have carried out the simulation for 1000 runs and presented the statistical results. Table I shows the TST results at three tumor growth stages for the two landscapes presented in Section II-C. It is obvious that WP-GSA performs better than the brute-force search at three tumor growth stages for the landscapes tested.

To demonstrate the effectiveness of the T-R principle proposed, we carry out the TST with a series of IA / UA durations between 0 and 40 seconds (i.e., $0 \leq \mathrm{T}_1 \leq 40$ s) and a constant IT duration of 20 s (i.e., $\mathrm{T}_2 = 20$ s). Thus, according to (6), the best IA / UA duration should be 10 s as $v_a = v_b = 30$ μm/s. The statistical results of the TST efficiencies at three tumor growth stages for two landscapes are shown in Fig. 6.

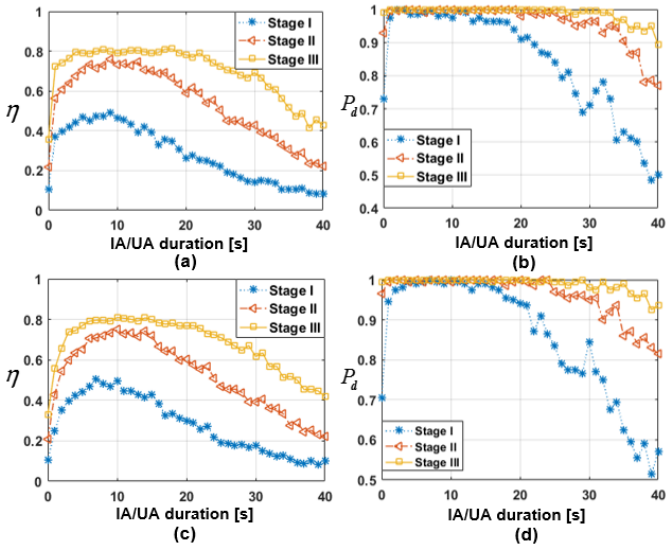

Fig. 6. Statistical results of the TST performances at three tumor growth stages for two landscapes. Landscape 1: (a) and (b); Landscape 2: (c) and (d).

It is obvious that when the IA/UA duration is 10 s, the TST performance is the best, which demonstrates the effectiveness of the T-R principle.

VII. Conclusion

We complete the TST by converting it into a computation process (i.e., *in vivo* computation). Considering the specific constraints of the nanorobots and landscape, we use the WP-GSA to realize the TST at three tumor growth stages for two representative BGF landscapes. Furthermore, we propose the T-R principle to overcome the issue of TST with unknown size. The statistical results of the TST performances at three tumor growth stages demonstrate the effectiveness of the T-R principle proposed.

Future work may include the validation of the proposed TST by real experiments to justify further its clinical relevance.

References

[1] A. Jemal, F. Bray, M. M. Center, J. Ferlay, E. Ward, and D. Forman, "Global cancer statistics," *CA: A Cancer J. Clinic.*, vol. 61, no. 2, pp. 69–90, 2011.

[2] A. A. Bharath, "Introductory medical imaging," *Syn. Lec. on Biomed. Eng.*, vol. 3, no. 1, pp. 1–186, 2008.

[3] V. A. Rahul, "A brief review on nanorobots," *SSRG-IJME*, vol. 4, pp. 15–21, 2017.

[4] A. Servant, F. Qiu, M. Mazza, K. Kostarelos, and B. J. Nelson, "Controlled in vivo swimming of a swarm of bacteria-like microrobotic flagella," *Adv. Mater.*, vol. 27, no. 19, pp. 2981–2988, 2015.

[5] A. A. Bui and R. K. Taira, *Medical imaging informatics*. Springer Sci. & Busi. Med., 2009.

[6] Y. Chen, S. Shi, X. Yao, and T. Nakano, "Touchable computing: computing-inspired bio-detection," *IEEE Trans. Nanobiosci.*, vol. 16, no. 8, pp. 810–821, 2017.

[7] Y. Chen, M. Ali, S. Shi, and U. K. Cheang, "Biosensing-by-learning direct targeting strategy for enhanced tumor sensitization," *IEEE Trans. Nanobiosci.*, 2019.

[8] J. B. Welsh, L. M. Sapinoso, S. G. Kern, D. A. Brown, T. Liu, A. R. Bauskin, R. L. Ward, N. J. Hawkins, D. I. Quinn, P. J. Russell, *et al.*, "Large-scale delineation of secreted protein biomarkers overexpressed in cancer tissue and serum," *Proc. Nat. Acad. Sci.*, vol. 100, no. 6, pp. 3410–3415, 2003.

[9] J. Ali, U. K. Cheang, Y. Liu, H. Kim, L. Rogowski, S. Sheckman, P. Patel, W. Sun, and M. J. Kim, "Fabrication and magnetic control of alginate-based rolling microrobots," *AIP Adv.*, vol. 6, no. 12, p. 125205, 2016.

[10] X. Yan, Q. Zhou, M. Vincent, Y. Deng, J. Yu, J. Xu, T. Xu, T. Tang, L. Bian, Y.-X. J. Wang, *et al.*, "Multifunctional biohybrid magnetite microrobots for imaging-guided therapy," *Sci. Robot.*, vol. 2, no. 12, p. eaaq1155, 2017.

[11] S. Shi, Y. Chen, X. Yao, and M. Zhang, "Lightweight evolution strategies for nanoswimmers-oriented in vivo computation," in *2019 IEEE Cong. Evol. Comp. (CEC)*, pp. 866–872, 2019.

[12] J. Holash, P. Maisonpierre, D. Compton, P. Boland, C. Alexander, D. Zagzag, G. Yancopoulos, and S. Wiegand, "Vessel cooption, regression, and growth in tumors mediated by angiopoietins and vegf," *Science*, vol. 284, no. 5422, pp. 1994–1998, 1999.

[13] Y. Gazit, J. W. Baish, N. Safabakhsh, M. Leunig, L. T. Baxter, and R. K. Jain, "Fractal characteristics of tumor vascular architecture during tumor growth and regression," *Microcirc.*, vol. 4, no. 4, pp. 395–402, 1997.

[14] J. W. Baish, Y. Gazit, D. A. Berk, M. Nozue, L. T. Baxter, and R. K. Jain, "Role of tumor vascular architecture in nutrient and drug delivery: an invasion percolation-based network model," *Microvas. Res.*, vol. 51, no. 3, pp. 327–346, 1996.

[15] R. King, "Theories and typologies of migration: an overview and a primer," *Malmö Inst. Stud. Migr., Div. Welf. (MIM).–Malmö*, 2012.